CIVIL ENGINEERING JOURNAL

Article no. 33

THE CIVIL ENGINEERING JOURNAL 4-2023

LIQUID-SOLID COUPLING RESPONSE OF SURROUNDING ROCK MASS OF LARGE-DIAMETER RIVER-CROSSING SHIELD TUNNEL

Shanglong Zhang[1], Xuansheng Cheng[2], Xiaoshuang Li[2], and Lei Qi[2]

1. *Hexi University, School of Civil Engineering, Department of Civil Engineering, Zhangye 734000, China; zsl889712@126.com*
2. *Lanzhou University of Technology, School of Civil Engineering, Department of Civil Engineering, Lanzhou, 730050, China*

ABSTRACT

The purpose is to investigate the response of the surrounding rock mass's seepage field, displacement field, and stress field during dynamic tunneling in soft soil. Relied on a large-diameter river-crossing shield tunnel project, considering driving force, shield tail grouting pressure, and the friction resistance between the shield shell and the soil, a three-dimensional fine tunnel model taking into account the liquid-solid coupling effect (LSCE) in the soil during dynamic tunneling was established by employing the finite difference method. The response characteristics of pore water pressure(PWP), displacement and stress in the surrounding rock mass were obtained. The results show that due to the liquid-solid coupling(LSC) in the surrounding rock mass, the PWP in the range of 0.5 times the hole diameter around the tunnel reduces and increases, respectively, during shield tunneling and shield tail grouting. The PWP of the soil close to the vault falls as the shield tunneling recedes, whereas the PWP close to the tunnel arch bottom rises. The impact range of shield tail grouting on the vertical settlement of the overlying soil is about 0.5 times the hole diameter. The shield tail grouting can significantly lessen the vertical settlement of the overlying soil and moderate the vertical uplift of the bottom soil. During shield tunneling the vertical stress distribution of the soil above the vault of the working position and around the excavation surface is funnel-shaped, and the vertical stress around the excavated tunnel decreases.

KEYWORDS

River-crossing tunnel, Dynamic tunneling, Liquid-solid coupling, Seepage field, Displacement field, Vertical stress

INTRODUCTION

With the advancement of urbanization, the problem of traffic congestion on the ground is becoming more and more prominent. Therefore, the development of underground traffic has become an important way to alleviate traffic congestion in large and medium-sized cities [1,2]. A great many river-crossing shield tunnels have been constructed or under construction along the river and coastal areas around the world, such as Seikan Tunnel (Japan), The Channel Tunnel (Britain and France), Jiaozhou Bay Undersea Tunnel (China), Cross Harbour Tunnel (Hong Kong), and Oujiang North Tunnel (China). Many challenges face the construction of a river-crossing shield tunnel under complex environmental conditions such as saturated soft soil, high water pressure and safety problems [3-5]. The shield tunneling will inevitably disturb the surrounding rock mass, and then the LSCE becomes obvious between soil particles and pore water. The PWP, displacement and stress of saturated soil are dynamically changed. Time-varying water-soil pressure severely affects the sealing of segments and the grouting quality behind the segments. In severe cases, it will threaten

the safe construction of shield tunnel, and the impact is particularly serious for large-diameter shield tunnel. Therefore, it is of great significance to explore the liquid-solid coupling response of saturated soft clay during dynamic tunneling of large-diameter river-crossing shield tunnels.

For the liquid-solid coupling response in the soil around the tunnel during the shield tunneling, researchers have conducted a lot of researches by employing theoretical analysis, numerical analysis and test methods, and fruitful results have been achieved. In terms of theoretical research, Zareifard and Fahimifar [6] analyzed the stability of underwater tunnel while taking the seepage force into account, and established the analytical solution of stress field and displacement field of surrounding rock mass of underwater tunnel. Wang et al. [7] considered the spatial variability of geotechnical parameters and applied random field theory to the reliability index analysis of ground settlement induced by the shield tunneling. According to the elastic-plastic theory, Pinto et al. [8] deduced the analytical solution of ground subsidence caused by shallow tunnel excavation in soft soil strata. Using the complex variable function theory, the distribution laws of the displacement, stress and PWP were obtained under the special conditions around the tunnel [9-12]. Taking the tunnel project in karst area of Dalian Metro Line 5 as the background, Zhang et al. [13] derived the linear relationship between $S_{max,0}/S_{max,z}$ and $(1-H_z/h)$ and its influence parameters based on the principle of similar soil loss. Using the multiple linear regression method, the prediction formula of the maximum ground subsidence caused by shield excavation under the condition of karst cave was established. Using extreme gradient boosting, artificial neural network, support vector machine, and multivariate adaptive regression spline, Zhang et al. [5] proposed a ground subsidence prediction model for EPB tunnel in Singapore. Ocak and Seker [14] employed artificial neural network, support vector machine and Gaussian processes to predict the ground settlement of Istanbul Metro tunnel excavated by earth pressure balance shield. However, in most theoretical methods the strata were regarded as homogeneous when studying the displacement field and PWP field during shield tunneling, and the influence of the actual multiple strata was not considered. Most methods are only applicable to specific conditions, and could not be widely used in the practical project due to the complexities of the ground conditions. In addition, numerical analysis is a favorite method for studying ground deformation caused by shield tunneling. Liu et al. [15] established a three-dimensional finite difference numerical model employing FLAC 3D, considering the factors such as trapezoidal support force, shield cone, trapezoidal grouting pressure, grouting body solidification, timely placement of lining, the soil settlement caused by shield tunnel excavation in silty sand stratum was studied. Using the discrete element method, Hu et al. [16] studied the surface and underground deformation characteristics of sandy soil under various burial depths and screw conveyor speeds. Based on the shield tunnel project in water-rich soft stratum, Li et al. [17] established a three-dimensional refined model considering fluid-solid coupling during shield tunneling, the effects of excavation face support pressure, friction between shield and soil, and synchronous grouting amount on ground settlement and structural deformation were mainly studied. To analyze the distribution of the stress field, displacement field, and PWP field in the soil during shield tunneling, numerical models with liquid-solid coupling were developed in the relevant literature [18-20]. Cheng et al. explored fluid-solid interaction response of subsea tunnel taking high water pressure [21] and under earthquake [22] into account. Yao et al. [23] studied the ground collapses in sand cobble strata caused by shield tunnel construction of Lanzhou Metro Line 1, divided the ground collapses into three types, A, B and C, and put forward corresponding control measures. Yuan et al. [24] used field monitoring to investigate the disturbance mechanism and the influence law on the surrounding rock soil in each stage of shield tunneling of a super-large diameter slurry shield tunnel. Using model test and finite element simulation, Shahin et al. [25] investigated the impact of ground overload and construction sequence on ground subsidence brought on by tunnel construction. Relied on Luoyang urban rail transit engineering, Wang et al. [26] conducted field tests in sandy cobble stratum, and studied the excavation disturbance and influence range of soil in each stage of earth pressure balance shield tunneling. Using numerical simulation, the disturbance characteristics of deformation, seepage and stress state of sandy cobble stratum during shield tunneling were obtained. Xie et al. [27] used the finite difference method to optimize the construction parameters of an EPB shield

tunnel, and validated the applicability of the numerical model of a large-diameter tunnel through field monitoring. However, in most numerical methods, the influence of liquid-solid coupling on seepage field and displacement field during dynamic shield tunneling was not considered, and most studies mainly focused on sandy soil strata, there were relatively few studies concentrating on dynamic tunneling in the silty soft soil strata with overlying water.

Relied on the large-diameter river-crossing shield tunnel project of S2 line of Wenzhou city railway, considering relevant parameters of shield tunneling, a fine numerical model considering the LSCE in the soil around the tunnel during dynamic excavating of a large-diameter river-crossing shield tunnel was established by employing finite difference method. The response characteristics of PWP, displacement and stress in the soil were obtained, and the influence of shield tail grouting on settlement characteristics and mechanical properties of strata during shield excavation was also analyzed. The findings of this research have significant theoretical implications for the construction of large-diameter river-crossing shield tunnels.

BASIC PRINCIPLE OF LIQUID-SOLID COUPLING

Seepage field equation of saturated soft soil

It is supposed that the flow of pore water in soil obeys Darcy's law. The compression of porous media follows the principle of Terzaghi effective stress. The seepage in soil is saturated flow. According to the porous media seepage theory, only considering the vertical compression, the three-dimensional seepage continuity equation of porous media single-phase fluid is as follows [28].

$$\frac{\partial}{\partial \mathrm{x}}\left(\frac{\rho K}{\mu}\frac{\partial p}{\partial x}\right)+\frac{\partial}{\partial \mathrm{y}}\left(\frac{\rho K}{\mu}\frac{\partial p}{\partial y}\right)+\frac{\partial}{\partial \mathrm{z}}\left(\frac{\rho K}{\mu}\frac{\partial p}{\partial z}\right)+\rho(\alpha+n\beta)\frac{\partial p}{\partial t}=0 \quad (1)$$

Where ρ is the fluid density, K is the permeability of porous media (m^2), μ is fluid viscosity (Pa·s), p is pore pressure (kPa), n is the porosity of porous media, t is time (s), a is compressibility coefficient of porous media $\alpha=-\frac{1}{V_b}\cdot\frac{dV_b}{dp}$, (1/kPa), β is coefficient of fluid compressibility $\beta=\frac{1}{\rho}\cdot\frac{d\rho}{dp}$, (1/kPa).

In the actual seepage, the source term w is considered to be added at the left of the above equation to obtain the basic seepage differential equation of single-phase fluid in compressible media.

$$\frac{\partial}{\partial \mathrm{x}}\left(\frac{\rho K}{\mu}\frac{\partial p}{\partial x}\right)+\frac{\partial}{\partial \mathrm{y}}\left(\frac{\rho K}{\mu}\frac{\partial p}{\partial y}\right)+\frac{\partial}{\partial \mathrm{z}}\left(\frac{\rho K}{\mu}\frac{\partial p}{\partial z}\right)+w+\rho(\alpha+n\beta)\frac{\partial p}{\partial t}=0 \quad (2)$$

The seepage field equation can be solved according to the constant pressure boundary condition or the constant flow boundary condition.

Displacement field equation of saturated soft soil

For small deformation, the fluid particle balance equation without considering the temperature effect is

$$-q_{i,\,j}+q_v=\frac{1}{M}\frac{\partial p}{\partial t}+\alpha\frac{\partial \varepsilon}{\partial t} \quad (3)$$

Where $q_{i,j}$ represents flow velocity of fluid, q_v represents fluid source intensity (1/s), M is biot modulus (N/m^2), a is biot coefficient, and ε is volume strain.

The variation of fluid pore pressure is caused by changes in the volume strain of the rock-soil mass. Meanwhile, changes in fluid pore pressure results in the variation of volume strain. The incremental form of the porous media constitutive equation can be expressed as

$$\Delta\tilde{\sigma}_{ij}+\alpha\Delta p\delta_{ij}=\hat{H}_{ij}(\sigma_{ij},\Delta\varepsilon_{ij}) \quad (4)$$

Where $\Delta\sigma_{ij}$ represents stress increment; H_{ij} represents a given function; ε_{ij} represents the total strain.

The compatibility equation can be used to characterize the relationship between strain rate and velocity gradient.

$$\dot{\varepsilon}_{ij}=\frac{1}{2}[\frac{\partial \dot{u}_i}{\partial x_j}+\frac{\partial \dot{u}_j}{\partial x_i}] \quad (5)$$

Where $\dot{u}$ represents velocity at some point in the medium.

The displacement field can be solved by knowing the surface displacement of rock and soil skeleton $u_{ij}=u_{ij}(x, y, z)$.

ENGINEERING CASE

Calculation parameters

Taking the river-crossing shield tunnel project of S2 line of Wenzhou city railway as the background, the project adopted the pressure balance shield machine with a diameter of 14900mm, which started from the Jiangnan working well and then advanced to the north, crossed the waters of Oujiang North Estuary, and reached the Jiangbei receiving well. The working diagram of mud balanced shield is shown in Figure 1. The tunnel lining ring has an outer diameter of 14500mm, an inner diameter of 13300mm, a ring width of 2000mm, and a segment thickness of 600mm.. The schematic diagram of shield tunneling across river is shown in Figure 2.

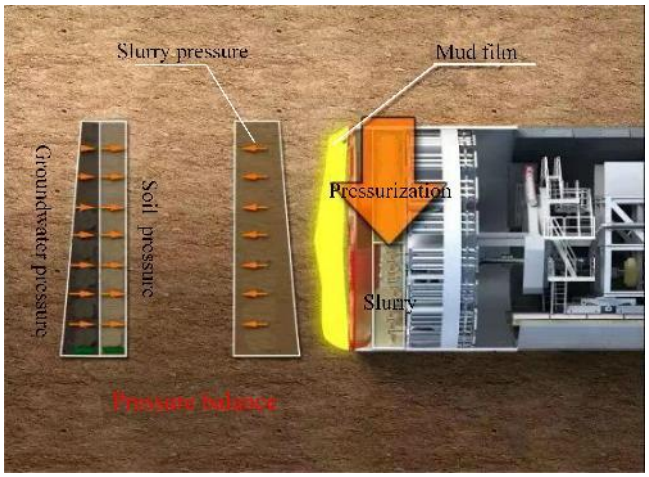

Fig. 1 –The working diagram of mud balanced shield.

Fig. 2 – Schematic diagram of shield tunneling across river

Table 1 displays the stratigraphic distribution and the parameters of a typical stratigraphic section. Affected by sea tide, the depth of the overlying water on the riverbed of Oujiang River is 8-16 m.

Tab. 1 - Lithologic parameters

Stratum	Moisture ratio under natural status /%	ρ/（kN/m³）	Es/MPa	φ/°	c/kPa	μ
Silt(1)	61.84	16.5	1.97	2.93	6.05	0.3
Silt(2)	56.34	16.8	2.09	3.11	6.38	0.3
Silt clay	50.05	17.3	2.5	3.89	6.24	0.32
Clay	40.46	18.4	3.6	4.12	6.76	0.35

The physical characteristics of the shield shell, lining, and grouting body are presented in Table 2. The lining structure's rigidity has been reduced to 85% of its original stiffness due to the impact of the staggered arrangement of segments and the segment joints.

Tab. 2 - Physical and mechanical parameters

	ρ/（kg/m³）	μ	E/MPa
Shield machine shell	7850	0.3	200000
Lining	2500	0.2	30600
Grouting body	2200	0.25	400

Computational model and boundary conditions

Employing the finite difference software FLAC3D, the calculation model of shield dynamic tunneling across river in multi-layer is established taking the liquid-solid coupling effect into account. Because of the structure's symmetry, half of the model is established for analysis. The model size is 65.45m×100m×78.2m based on the actual project size and taking the influence of the boundary effect into account, as shown in Figure 3. The water level above the riverbed is 12 m. The length of the shield machine is selected as 6 m. According to the technical data of the project, the weight of the shield machine is 1655 t. The lining segment has a width of 2 m, a thickness of 0.6 m, and the thickness of the grouting layer behind the lining ring is 0.2m. The surrounding rock mass and grouting layer adopt an 8-node solid element, and the lining and shield shell adopt shell element. The following are the boundary conditions: The upper surface of the model is subjected to 120 MPa pore water pressure and 120 MPa vertical force. The horizontal displacements on the model's four sides are constrained, as is the vertical displacement at the bottom. The model's four sides and the bottom have impermeable boundaries.

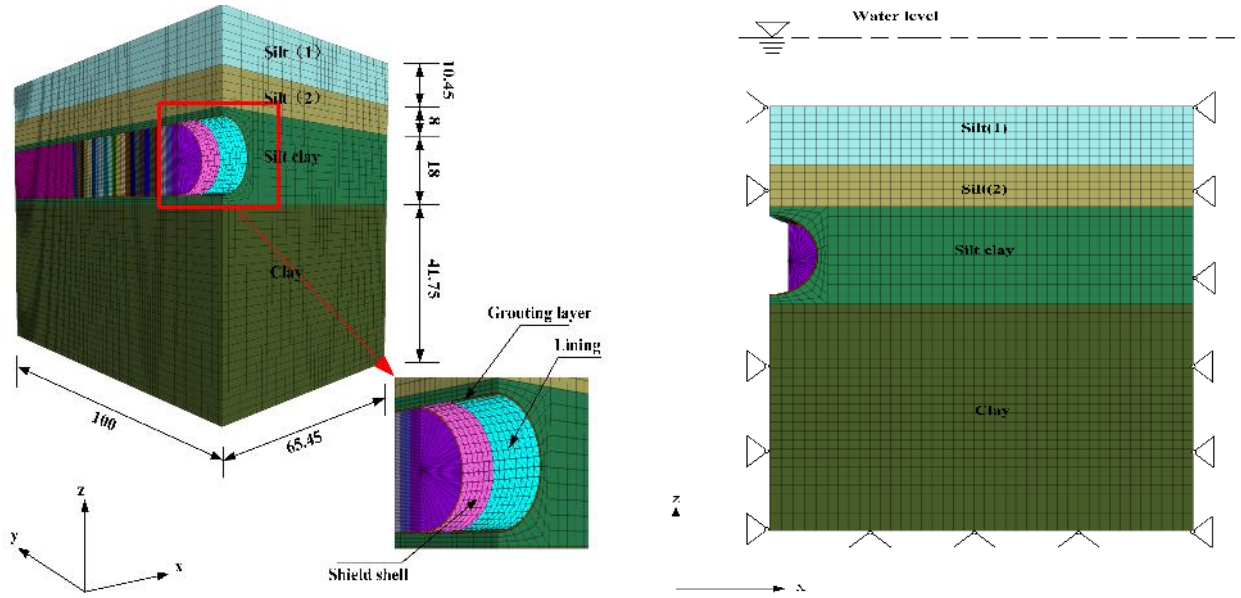

(a) Integral model of shield tunnel (b) Boundary constraints of shield tunnel

Fig. 3 – Schematic diagram of river-crossing tunnel model

Numerical procedure

For the soil, the Mohr-Coulomb (M-C) criterion is chosen, and the elastic model is applied to the lining segment and the shield shell. The total overburden pressure is chosen in the calculation.

To mimic the consolidation settlement of underwater strata prior to tunnel excavation, the ground stress balancing is performed, and at this point, the PWP in the soil is treated as hydrostatic pressure.

In the numerical simulation of shield tunneling across river, the shield machine advances 2 meters for each excavation ring. According to the monitoring data of the practical project, the tunneling speed of the river-crossing shield tunnel is low, which is 6-8m/d. In addition, the supporting pressure on the excavation face is constant, which is simulated as the surface load distributed along the depth trapezoid, so the tunneling speed is considered to be constant. Therefore, the influence of tunneling speed on the surrounding rock soil is not considered in this paper. The supporting pressure acting at the tunnel surface center is obtained by Equation (6), and the gradient pressure is acted on the tunnel surface. The tail grouting pressure is set as 0.5273MPa according to the water-soil pressure around the hole. Considering the condensation and hardening of shield tail grouting is completed within 8~11 hours, and the excavation of one ring is completed within about 6 hours, it is assumed that the shield machine excavates two rings during this period. To simplify the calculation, the grouting pressure of the former ring on the surrounding rock soil and lining segment is considered as 0.2637MPa when the shield tail grouting of back ring is carried out [29]. The friction resistance between the shield shell and the soil is calculated by Equation (7), which is 159132N/m^2. By using a method in which fluid calculations and solid mechanics calculations are performed simultaneously, the liquid-solid coupling effect is obtained during shield tunneling across river.

$$\sigma_x=\sigma_y=[k_0\rho_d+(k_0(n-1)+1)\rho_w]gh \quad (6)$$

Where, k_0 is the lateral pressure coefficient, and n is the porosity. Based on the results of engineering geological investigation, k_0 is 0.674, and n is 0.51.

$$F_1=\frac{1}{4}\times(p_0+p_{01}+p_1+p_2)\cdot u \quad (7)$$

$$p_{01}=p_0+W/(D\cdot L) \quad (8)$$

$$p_1=p_0\cdot k_0 \quad (9)$$

$$p_2=(p_{01}+\gamma'\cdot D)\cdot k_0 \quad (10)$$

where, p_0 is the soil's vertical force at the top of the shield machine, p_{01} is the soil's vertical force at the bottom of the shield machine, p_1 is the lateral force at the top of the tunnel, p_2 is the lateral force at the bottom of the tunnel, D is the shield machine's outer diameter, L is its length, u is the friction coefficient between the soil and the steel body, and u is 0.3.

To avoid the effect of boundary conditions on the seepage, displacement and stress in the soil around underwater tunnel, the 29m section of the 15th ring in the middle of the tunnel was taken as the analysis section, and the measuring points were arranged on this section. It is assumed that the shield machine has completed the excavation of the first three rings at the beginning, and the soil is in a stable state.

LIQUID-SOLID COUPLING RESPONSE OF SURROUNDING ROCK SOIL

Pore water pressure analysis

Figures 4 and 5 show the variation laws of PWP at measuring points with shield tunneling from the fourth ring to the 24th ring. Measuring points are arranged at different radius (7.45m, 8.45m, 9.45m, 10.45m, 11.45m, 12.45m, 13.45m, 14.45m, 15.45m) along 45° direction between arch waist and vault of the tunnel in 29m section of the 15th ring in Figure 4. In Figure 5, measuring points are arranged at different heights (7.45m, 8.45m, 9.45m, 10.45m, 11.45m, 12.45m, 13.45m, 14.45m, 15.45m) above the tunnel vault in 29m section of the 15th ring. It can be seen from the figures that during the shield tunneling from the 14th to the 17th ring, owing to the continuous disturbance to the soil of the analysis section, the stress of the surrounding soil releases, the PWP of the measuring points around the tunnel in a certain range of the analysis section is reduced because of the decrease

of porosity and permeability. And the PWP of the measuring points in this range dropped most during the excavation of the 17th ring. As the shield machine excavates to the 18th ring, at this time the shield tail grouting of the 15th ring is carried out. Due to the reinforcement effect of grouting pressure and grouting amount on the soil, the PWP at the measuring points of the analysis section rises sharply. During the excavation of the 19th ring, the grouting in the 15th ring has not been completely solidified and hardened, and there is still a certain grouting pressure on the soil. The PWP at the measuring points in the surrounding rock soil decreases to a certain extent, but it is generally higher than that of the 17th ring tunneling. After that, the PWP of the measuring points gradually become stable. From Figures 4 and 5, it can be concluded that the impact range of the PWP in surrounding rock soil around the tunnel during the underwater shield tunneling is about 0.5R (R is the outer diameter of the shield tunnel).

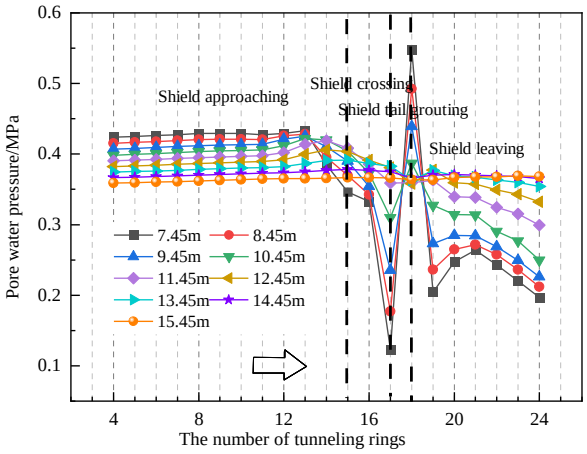

Fig. 4 – Pore water pressure of measuring points along 45°direction

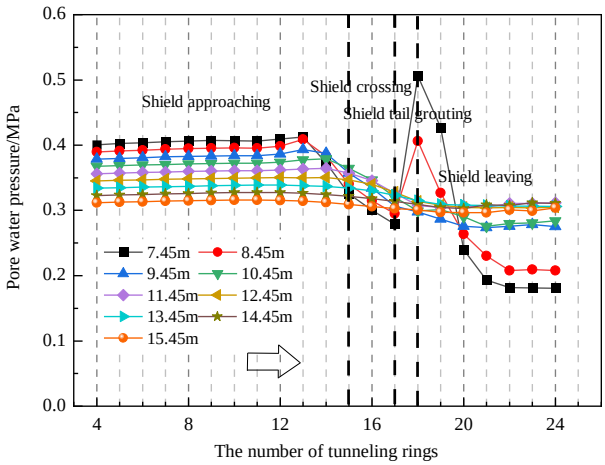

Fig. 5 – Pore water pressure of vertical measuring points above tunnel vault

Figures 6(a) and 6(b) show the PWP distribution of the longitudinal section containing the tunnel axis and the monitoring cross section when the shield machine excavates to the 16th and the 18th ring, respectively. It can be obtained from Figure 6(a) that when the shield tunneling reaches the 16th ring, because of the disturbance to the soil in a certain range around the tunnel, the effective stress of the soil in this range is released. And there is a significant liquid-solid coupling in the soil, which lowers the PWP in this range. It can be obtained from Figure 6(b) that when the shield tunneling reaches the 18th ring, the shield tail grouting of the 15th ring is carried out. The effective stress of soil particles increases in a certain range around the tunnel, the soil particles undergo compression deformation, and the liquid-solid coupling raises the PWP.

The distribution of PWP on the longitudinal section containing the tunnel axis is roughly similar when the shield reaches the 16th and the 18th ring. In the completed construction section (1-12 rings in Figure 6(a), 1-14 rings in Figure 6(b)), the PWP in the soil near the vault decreases and increases near the tunnel arch bottom. The reason is that with the solidification and hardening of the grouting body, the soil above the vault sinks under the vertical water-soil pressure, and the effective stress of soil particles increases. The soil under the tunnel arch bottom uplifts, and the effective stress decreases. Under the assumption that the total stress of the soil remains constant, the PWP in the soil above the vault decreases, while the PWP in the soil near the tunnel arch bottom increases. So, tunnel anti-floating measures such as secondary grouting should be taken during construction. Furthermore, the PWP distribution around the excavation surface is funnel-shaped. To summarize, it is suggested that the PWP in the surrounding rock mass be regarded as dynamic water pressure caused by the liquid-solid coupling in the underwater shield tunnel construction.

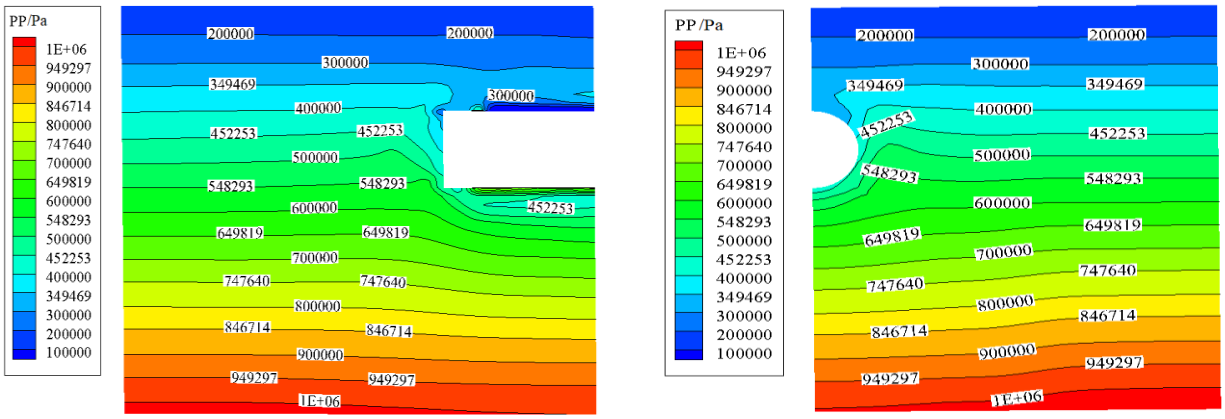

(a) PWP when shield crossing

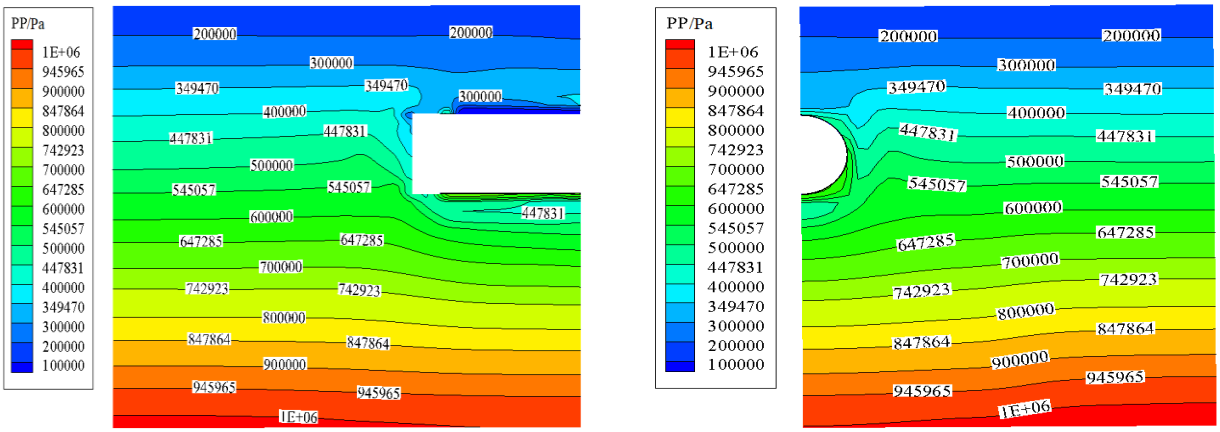

(b) PWP when shield tail grouting

Fig. 6 – PWP of monitoring section

Displacement field analysis

Vertical displacement during shield tunneling

Figure 7 presents the variation laws of vertical displacement at measuring points with shield tunneling from the fourth ring to the 24th ring. Measuring points are arranged at different heights (7.45m, 8.45m, 9.45m, 10.45m, 11.45m, 12.45m, 13.45m, 14.45m, 15.45m) above the tunnel vault in 29m section of the 15th ring. The vertical subsidence of the monitoring point decreases as the distance between the monitoring point and the tunnel axis increases above the tunnel vault. When the shield machine excavates to the 8th ring, the small vertical settlement of the monitoring point above the vault of the 15th ring analysis section begins to produce. After that, with the shield machine excavating forward the disturbance to the monitoring section increases, and the vertical settlement of the monitoring point continues to increase. It shows that the influence range of the underwater shield tunneling on the vertical displacement of the front surrounding rock soil is about 1R. From the 14th ring to the 17th ring, with the continuous shield tunneling, the vertical displacement of the monitoring points continues to increase due to the release of soil stress caused by the disturbance to the soil of the analysis section. When the shield tunnel is excavated to the 18th ring and the 19th ring the vertical displacement growth of the monitoring points tends to be gentle due to the reinforcement effect of the grouting pressure and grouting amount behind the 15th ring segment. The maximum vertical settlement of the vault measuring point (0,29,7.45) is 14.88mm. According to the excavation of the 20th and subsequent rings, the influence range of the synchronous grouting of the shield tail on the vertical settlement of the surrounding rock soil above the vault is approximately 0.5R

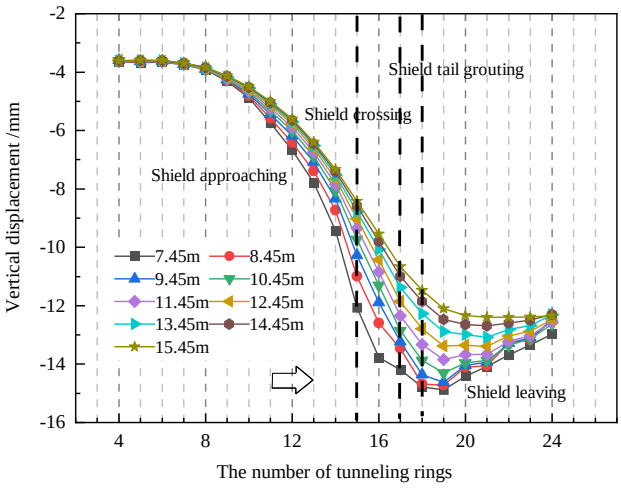

Fig. 7 – Vertical displacement of measuring points above tunnel vault

Figure 8 presents the vertical displacement distribution of the longitudinal section containing the tunnel axis and the monitoring cross section when the shield machine excavates to the 18th ring. It can be concluded that the LSCE in the soil is obvious during the underwater tunnel excavation, and the distribution of vertical displacement in surrounding rock mass is complex, especially around the tunnel. With the shield machine moving forward, the arch bottom of the tunnel uplifts and the vault sinks. Due to the grouting amount and grouting pressure behind the 15th ring lining segment, the vertical displacement of the soil above the 15th ring segment is significantly reduced. The local surrounding rock soil at the tunnel's bottom in front of the excavation face has a slight upward uplift, indicating that the slurry pressure on the excavation surface should be controlled to avoid excavation surface instability during the shield tunnel construction.

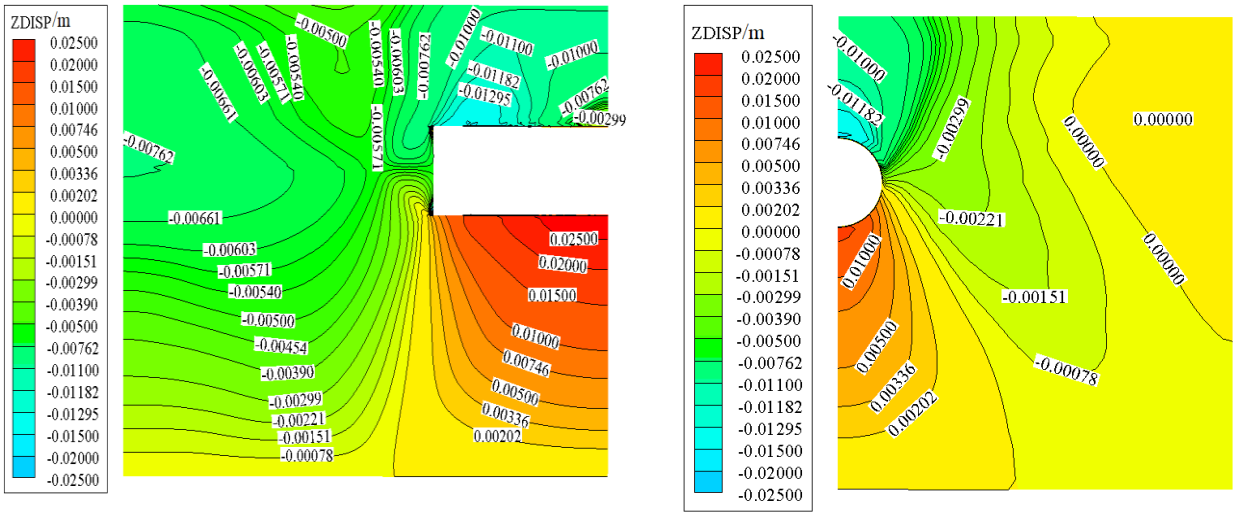

Fig. 8 – Vertical displacement when shield tail grouting

Strata settlement

Figure 9 presents the vertical settlement of different strata above the vault of the tunnel in the 29 m monitoring section of the 15th ring when tunneling in the 19th ring. It can be obtained that the maximum ground subsidence occurs at the upper part of the shield tunnel axis, and with the increase of stratum depth, the vertical settlement above the axis of the tunnel is larger. The shape of the settlement curve of each stratum is similar, and all conform to the Gaussian normal distribution of Peck curve. The deeper the depth of the stratum, the narrower the settlement trough width, indicating

that the disturbance range of the soil is smaller. This is consistent with the conclusions of existing studies, and also proves the correctness and reliability of the numerical analysis method in this paper.

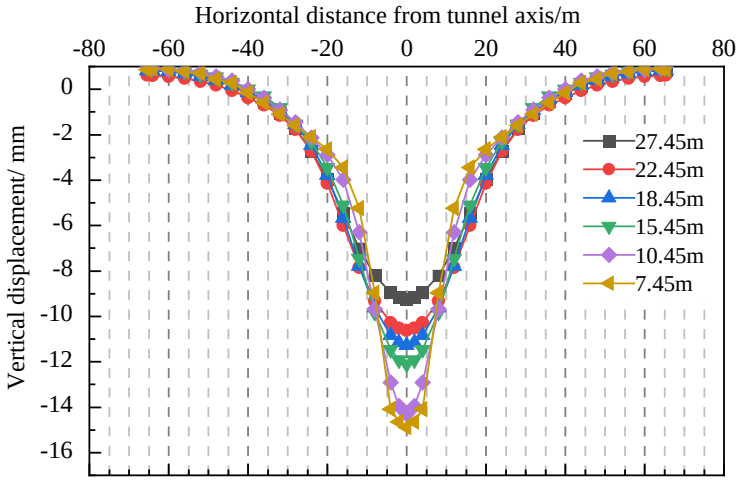

Fig. 9 – Vertical settlement of different strata

Vertical settlement of tunnel vault and arch bottom

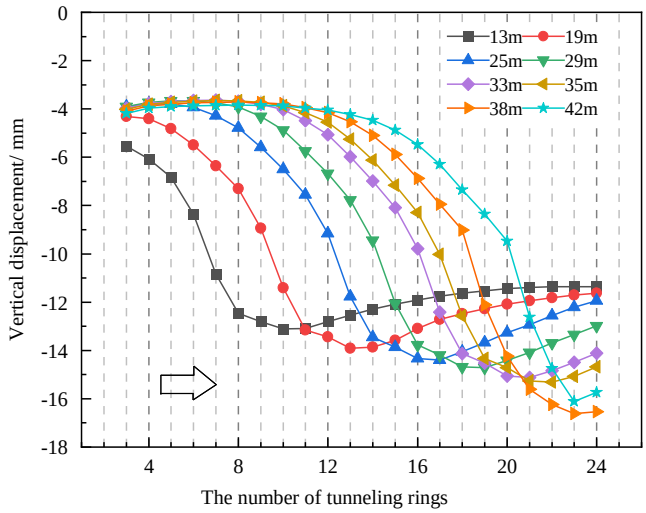

Fig. 10 – Vertical displacement of measuring points at tunnel vault

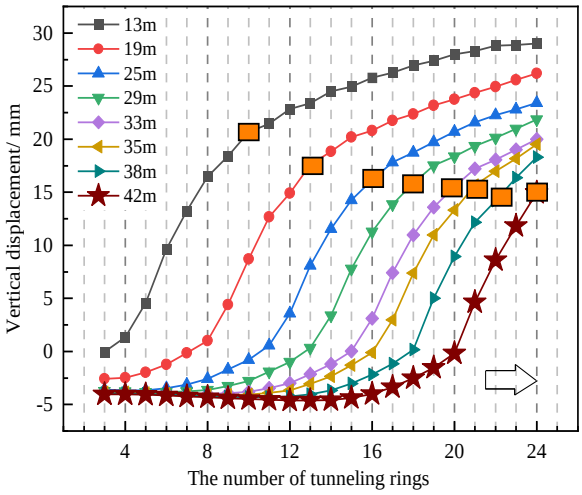

Fig. 11 – Vertical displacement of measuring points at arch bottom of tunnel

Figures 10 and 11 show the relation curves between the vertical displacements of the measuring points and the number of tunneling ring along the tunnel excavation direction. The measuring points are located at the top and bottom of the tunnel at 13m, 19m, 25m, 29m, 33m, 35m, 38m, and 42m, respectively. It can be obtained from the figure that the support of each lining segment and the grouting significantly reduce the vertical settlement rate of the vault and the vertical uplift rate of the arch bottom, which indicates that the shield tail synchronous grouting can effectively reinforce the surrounding rock soil. The displacement of the tunnel vault and arch bottom is typically stable while the shield machine advances. The final settlement of the tunnel vault is about 11.35 mm, and the uplift of the arch bottom's uplift is about 28.97 mm.

Vertical stress analysis

Figure 12 shows the distribution of vertical stress on the longitudinal section along the tunnel axis and the monitoring cross section at the 29m section of the 15th ring in different stages of underwater shield tunneling. In different rings tunneling, the vertical stress distribution of the longitudinal section is basically similar. Due to the disturbance and stress release of the surrounding rock mass, the shield machine's continued forward motion significantly reduces the vertical stress of the soil surrounding the excavated tunnel. With the continuous advance of shield tunneling, the vertical stress around the tunnel tends to be stable, which is generally smaller than the initial stratum stress. It is advantageous for the safe operation of the shield tunnel in the later period. The vertical stress of the soil above the vault at the working position of the shield machine and at the excavation face presents a funnel-shaped distribution. For the vertical stress distribution of the monitoring cross section in different tunneling stages, in Figure 12(a), the shield tunneling has not reached the monitoring section, due to the disturbance to the front soil, the vertical stress of the front soil is released and reduces. In Figure 12(b), the shield machine crosses the monitoring section as the shield tunneling reaches the 16th ring. The soil around the monitoring section is disturbed, and the vertical force of the soil around the tunnel further reduces compared with the 13th ring. In Figure 12(c), the shield tunneling reaches the 18th ring, and the tail grouting is carried out behind the 15th ring segment. The vertical stress of the soil on the upper part of the arch waist around the tunnel of the monitoring section continues to decrease, and the stress reduction range is greater than that of the 16th ring. The vertical stress of the soil at the lower part of the arch waist increases compared with that of the 16th ring, which indicates that the shield tail grouting can effectively resist floating. When the shield machine excavates to the 21st ring, far from the monitoring section, as shown in Figure 12(d), the vertical stress of the monitoring section gradually becomes stable.

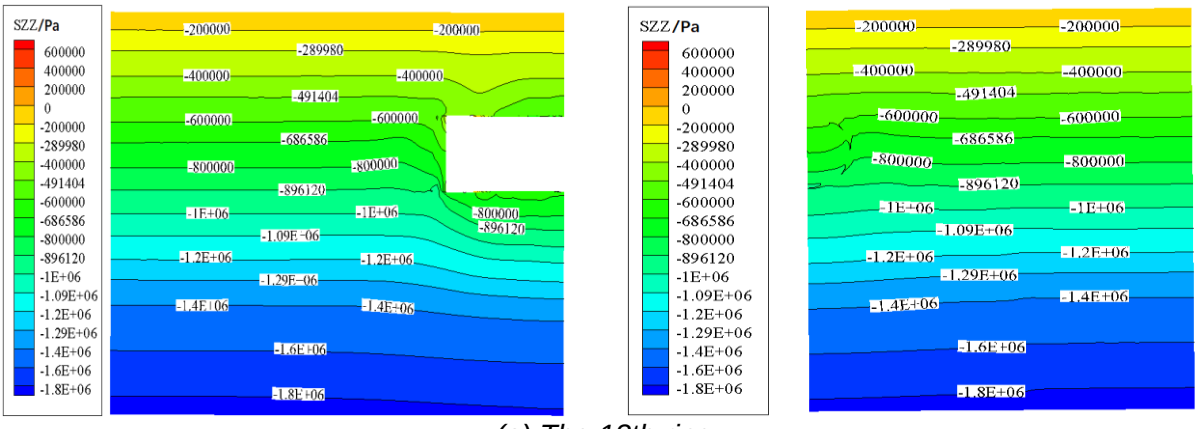

(a) The 13th ring

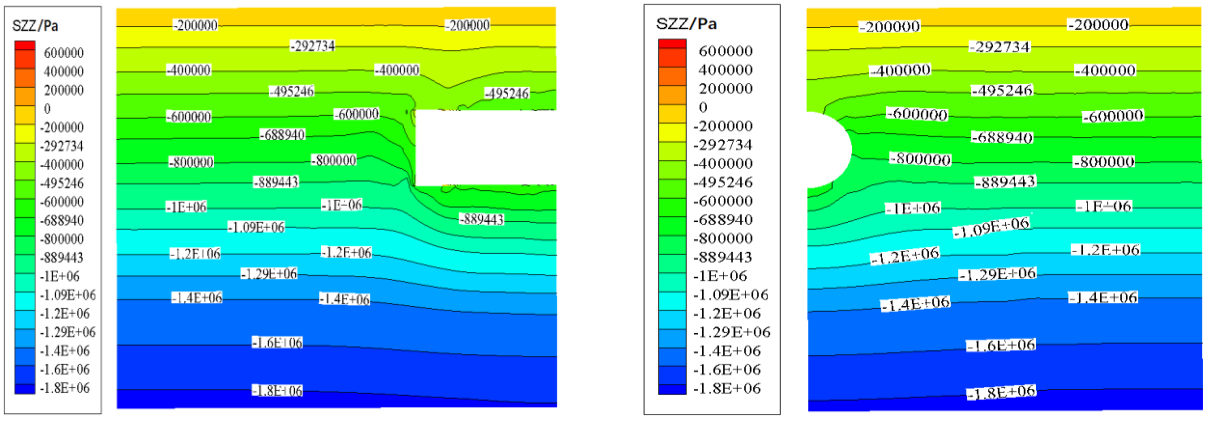

(c) The 16th ring

Fig. 12 – Vertical stress of monitoring section

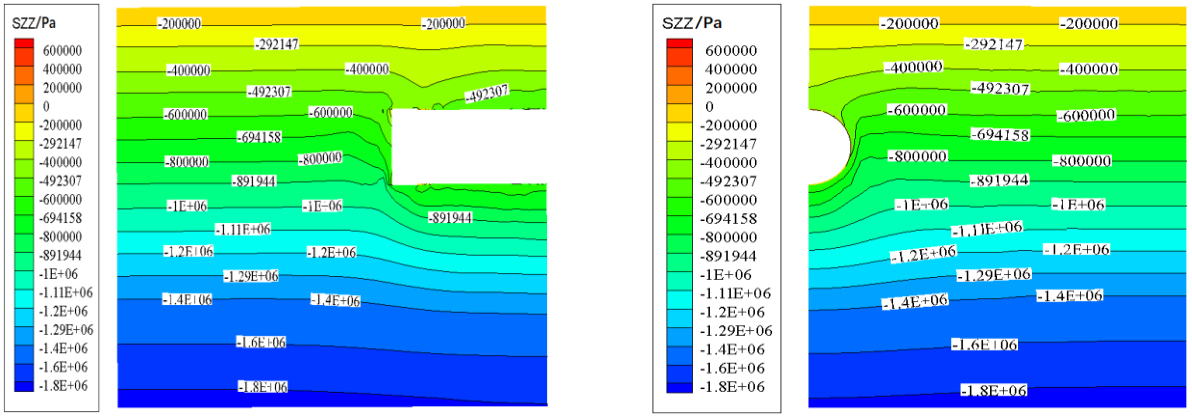

(d) The 18th ring

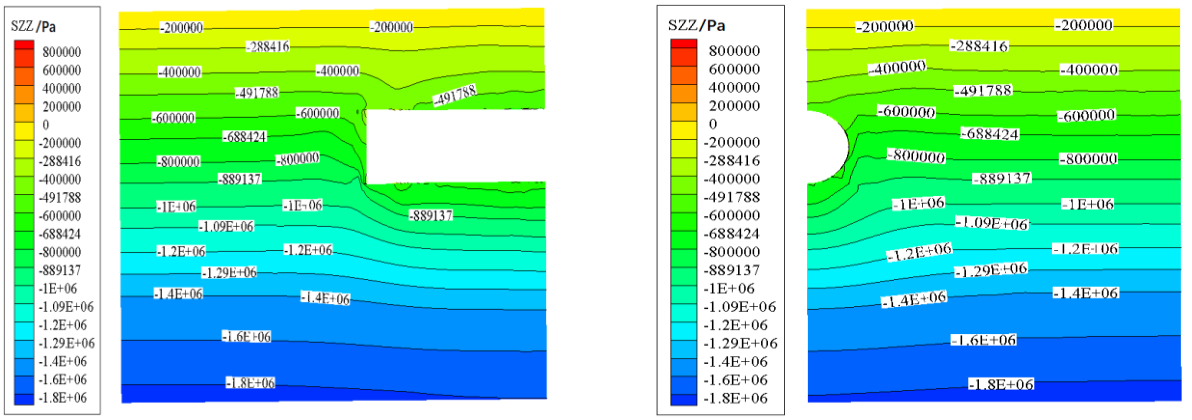

(e) The 21st ring

Fig. 12 – Vertical stress of monitoring section

CONCLUSIONS

(1) During the underwater shield tunneling and the shield tail grouting, the PWP in the range of 0.5R around the tunnel reduces and increases respectively due to the liquid-solid coupling. When the shield moves away, the PWP of the soil near the tunnel vault decreases, and grows near the arch bottom of the tunnel, the tunnel anti-floating measures such as secondary grouting should be taken. The PWP in the surrounding rock soil should be regarded as hydrodynamic pressure in the construction of an underwater large-diameter shield tunnel.

(2) The influence range of underwater shield excavating on the vertical displacement of the front soil is about 1R. Due to stress release, the vertical settlement of the surrounding soil above the vault increases as the shield approaches the monitoring section. The reinforcement effect of shield tail grouting behind the lining segment can effectively reduce vault soil vertical subsidence and slow down arch bottom soil uplift. The influence range of shield tail grouting on the vertical subsidence of the soil above the vault is about 0.5R.

(3) The deeper the burial depth of the stratum, the narrower the ground subsidence trough and the smaller the ground disturbance range. The local soil at the bottom of the tunnel in front of the excavation surface uplifts, indicating that the slurry pressure on the excavation surface should be controlled to avoid the instability of the excavation surface during the tunneling.

(4) The vertical stress of the soil surrounding the tunnel reduces during the excavation of the shield, and the vertical stress of the soil above the vault of the working position of the shield machine and around the excavation face is funnel-shaped distribution due to the influence of liquid-solid coupling. After the vertical stress around the excavated tunnel tends to be stable, the vertical stress

is generally lower than the initial formation stress, which is advantageous for the safe operation of the shield tunnel in the later stage.

ACKNOWLEDGMENTS

This research is supported in part by the National Natural Science Foundation of China (Grant No. 52178389), the Science and Technology Planning Project of Zhejiang Traffic Quality Supervision Industry (Grant No. ZJ201906).

REFERENCES

[1] Zhang Z.G., Huang M.S., Pan Y.T., et al., 2021. Analytical prediction of time-dependent behavior for tunneling-induced ground movements and stresses subjected to surcharge loading based on rheological mechanics. Computers and Geotechnics, Vol.129: 103858. https://doi.org/10.1016/j.compgeo.2020.103858

[2] Liang Y., Chen X.Y., Yang J.S., et al., 2020. Analysis of ground collapse caused by shield tunnelling and the evaluation of the reinforcement effect on a sand stratum. Engineering Failure Analysis, Vol. 115: 1-15. https://doi.org/10.1016/j.engfailanal.2020.104616

[3] Zhang S.L., Cheng X.S., Qi L., et al., 2022. Face stability analysis of large diameter shield tunnel in soft clay considering high water pressure seepage. Ocean Engineering, Vol.253: 111283. https://doi.org/10.1016/j.oceaneng.2022.111283

[4] Pan Q.J., Dias D., 2018. Three dimensional face stability of a tunnel in weak rock masses subjected to seepage forces. Tunnelling and Underground Space Technology, Vol.71, 555-566. https://doi.org/10.1016/j.tust.2017.11.003

[5] Zhang J. S., Xu M. Y., Cui M. H., et al., 2022. Prediction of ground subsidence caused by shield tunnel construction under hidden karst cave. Geotechnical and Geological Engineering, Vol.40: 3839-3850. https://doi.org/10.1007/s10706-022-02136-3

[6] Zareifard M.R., Fahimifar A., 2016. A simplified solution for stresses around lined pressure tunnels considering non-radial symmetrical seepage flow. KSCE Journal of Civil Engineering, Vol.20: 2640-2654. https://doi.org/10.1007/s12205-016-0105-5

[7] Wang C.H., Zhu H.H., Xu Z.C., et al., 2018. Ground surface settlement of shield tunnels considering spatial variability of multiple geotechnical parameters. Chinese Journal of Geotechnical Engineering, Vol.40:270-277. https://doi.org/10.11779/CJGE201802007

[8] Pinto F., Zymnis D.M., Whittle A.J., 2014. Ground movements due to shallow tunnels in soft ground. II: Analytical interpretation and prediction. Journal of Geotechnical and Geoenvironmental Engineering, Vol. 140, 80-90. https://doi.org/10.1061/(ASCE)GT.1943-5606.0000947

[9] Wang L.Z., Lv X.J., 2007. A complex variable solution for different kinds of oval deformation around circular tunnel in an elastic half plane. Chinese Journal of Geotechnical Engineering, Vol.29:319-327. https://doi.org/10.1016 / S1874-8651(08)60042-3

[10] Huangfu M., Wang M.S., Tan Z.S., et al., 2010. Analytical solutions for steady seepage into an underwater circular tunnel. Tunnelling and Underground Space Technology, Vol.25:391-396. https://doi.org/10.1016/j.tust.2010.02.002

[11] Song H.R., Zhang D.L., Fang Q., 2015. Analytic solution on the stress of surrounding rocks for shallow subsea tunnel. China Civil Engineering Journal, Vol.48: 283-288 https://doi.org/CNKI:SUN:TMGC.0.2015-S1-048

[12] Wu Z.S., Liu X.R., Liang B., et al., 2014. Study of seepage property and calculated watershed around underwater tunnels. Chinese Journal of Rock Mechanics and Engineering, Vol.33:2402-2408. https://doi.org/10.13722/ j.cnki.jrme.2014.12.005

[13] Zhang W. G., Li H. R., Wu C. Z., et al., 2019. Soft computing approach for prediction of surface settlement induced by earth pressure balance shield tunneling. Underground Space, 1-29. https://doi.org/10.1016/j.undsp.2019.12.003

[14] Ocak I., Seker S.E., 2013. Calculation of surface settlements caused by EPBM tunneling using artificial neural network, SVM, and Gaussian processes. Environmental Earth Sciences, Vol. 70: 1263-1276. https://doi.org/ 10.1007/s12665-012-2214-x

[15] Liu C.L., Yang S.Y., Liu W.J., et al., 2022. Three-dimensional numerical simulation of soil deformation during shield tunnel construction. Mathematical Problems in Engineering, Vol. 2022: 1-11. https://doi.org/10.1155/2022/5029165

[16] Hu X.Y., He C., Lai X.H., et al., 2020. A DEM-based study of the disturbance in dry sandy ground caused by EPB shield tunneling. Tunnelling and Underground Space Technology, Vol.101: 1-16. https://doi.org/10.1016/j.tust.2020.103410

[17] Li X.Y., Zhang D.L., Hou Y.J., 2022. Analysis of shield tunnel ground deformation characteristics and affecting factors in water-rich soft stratum: A case study on the section tunnel of Tianjin Metro Line 6. Applied Sciences. Vol. 12: 1-22. https://doi.org/10.3390/app12126208

[18] Jin X.G., Li X.H., Zhang Y.Q., 2010. Seepage-stress coupling analysis of rive-crossing tunnel excavating. Hydrogeology & Engineering Geology, Vol.37: 62-67.https://doi.org/10.3969/j.issn.1000-3665.2010.01.013

[19] Ji Y.J., Liu J.J., Cheng L.S., 2011. Numerical simulation of tunnel excavation considering fluid solid coupling. Rock and Soil Mechanics, Vol.32: 1229-1233. https://doi.org/10.4028/www.scientific.net/AMR.211-212.106

[20] Wang C., 2018. Disturbance analysis of shallow buried and small interval shield tunnel excavation based on fluid-solid coupling. Subgrade Engineering, Vol.4:40-44.

[21] Cheng X.S., Zhang S.L., Qi L., et al., 2021. Fluid-solid coupling response of shield tunnel lining structure under high water pressure. Marine Georesources & Geotechnology, 1-11. https://doi.org/10.1080/1064119X.2021.1971805.

[22] Cheng X.S., Xu W.W., Yue C.Q., et al., 2014. Seismic response of fluid-structure interaction of undersea tunnel during bidirectional earthquake. Ocean Engineering, Vol.75:64-70. https://doi.org/10.1016/j.oceaneng. 2013.11.017

[23] Yao Q.Y., Di H.G., Ji C., et al., 2020. Ground collapse caused by shield tunneling in sandy cobble stratum and its control measures. Bulletin of Engineering Geology and the Environment. Vol. 79: 1-16. https://doi.org/10.1007/s10064-020-01878-9

[24] Yuan D.J., Yin F., Wang H.W., et al., 2009. Study of soil disturbance caused by super-large diameter slurry shield tunnelling. Chinese Journal of Rock Mechanics and Engineering, Vol.28:2074-2080. https://doi.org/10.3321/j.issn:1000-6915.2009.10.015

[25] Shahin H.M., Nakai T., Hinokio M., et al., 2004. Influence of surface loads and construction sequence on ground response due to tunnelling. Soils and Foundations, Vol.44: 71-84. https://doi.org/10.3208/sandf.44.2_71

[26] Wang W., Liu J.J., Zhang X.M., et al., 2022. Researches on the excavation disturbance of shield tunnel in sandy cobble ground. Geofluids, Vol. 2022: 1-15. https://doi.org/10.1155/2022/2373133

[27] Xie X.Y., Yang Y.B., Ji M., 2016. Analysis of ground surface settlement induced by the construction of a large-diameter shield-driven tunnel in Shanghai. Tunnelling and Underground Space Technology, Vol.51: 120-132. https://doi.org/10.1016/j.tust.2015.10.008

[28] Yuan L.J., Li Z.Q., Wu S.Z., et al., 2001. Mechanics of engineering seepage and its application. China Building Materials Industry Press, Beijing, China.

[29] Yu L.B., 2018. Study on the seepage field variation and soil deformation caused by synchronous grouting of large diameter shield machine during the construction of a tunnel. Master's thesis, South China University of Technology, Guangzhou, China.